The Structure of a Fair Weather Boundary Layer Based on the Results of Several Measurement Strategies

GARY BARNES AND GEORGE D. EMMITT

University of Virginia, Department of Environmental Sciences, Charlottesville, VA 22903

BURGHARD BRUMMER

Max-Planck-Institut fur Meteorologie, Hamburg, Federal Republic of Germany

MARGARET A. LEMONE

National Center for Atmospheric Research[1], Boulder, CO 80307

STEPHEN NICHOLLS

Meteorological Research Flight, Royal Aircraft Establishment, Farnborough, U.K.

(Manuscript received 15 February 1979, in final form 8 November 1979)

ABSTRACT

A fair weather boundary layer (BL) with light winds and scattered cumulus to 1100 m is examined in the GATE C-scale triangle using data from tethered balloons, surface measurements from the booms of the ships, structure sondes and gust probe aircraft. The original goal was a comparison of the instrumentation in an expected uniform field of wind, temperature and humidity. It became rapidly obvious that nonuniformities existed not only at the turbulence scales (a few meters to 1 km) but also on scales 10 km and larger. Thus the goal evolved into 1) combining the observations to present a coherent picture of the day, 2) putting the results of various observational techniques in perspective and 3) examining the nonuniformity.

Different aspects of the day are revealed by the different observational techniques. The *Dallas* tethered balloon reveals a noticeable modification of the BL nearly coincident with a change in convective activity. In spite of nonuniformity, and the interception of convective events similar to that at the *Dallas*, the flux profiles from aircraft show that the BL behaves in a similar way to those reported previously near "horizontally homogeneous" conditions. Moisture and energy budgets performed for this day show the expected convergence of sensible and latent heat in the boundary layer but in a shallower layer than expected.

1. Introduction

During the GATE Workshop (NSF/NCAR, 1977), the authors of this paper presented considerable data on the fair weather boundary layer. During the discussions it was difficult to get a consistent picture. Many investigators complained of difficulties using the data from the diverse sets of instrumentation deployed in the GATE experiment or even independent measurements from similar instruments—even after careful intercomparison and calibration. The authors decided to combine their observations and analysis techniques to analyze a very suppressed day when horizontally homogeneous conditions would insure easy comparison of both instrumentation and of observational techniques. The day selected was 10 September, a day with scattered cumulus with tops to 1100 m and southwesterly winds of ~3 m s^{-1}. The observations were to be combined to extract a consistent case study and resolve the differing interpretations of GATE fair weather data. Instead, the resulting case study revealed a complex fair weather boundary layer. Nonuniformities existed not only on the accepted subcloud layer turbulence scale (<1 km) and the synoptic scale (~1000 km) but also there was well-defined structure on the mesoscale (~10 km) with sufficient amplitude to make determination of synoptic gradients difficult. However, the mixed-layer temperature and humidity flux profiles are nearly linear, and the turbulence kinetic energy budget shows near equilibrium—both results "typical" for a fair weather day.

[1] The National Center for Atmospheric Research is sponsored by the National Science Foundation.

0027-0644/80/030349-16$08.00
© 1980 American Meteorological Society

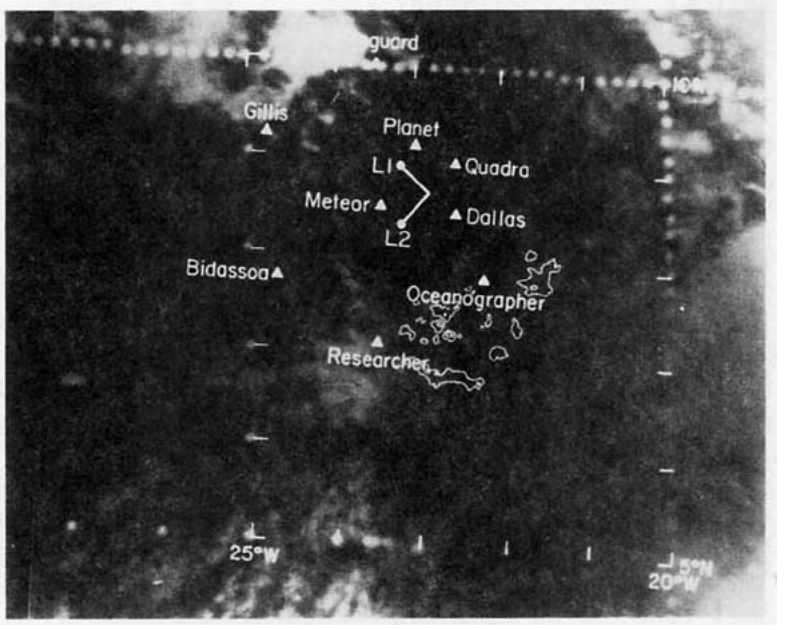

FIG. 1. 1500 GMT satellite picture (1 nm resolution) centered on the GATE array. The C-scale triangle formed by the *Dallas*, *Meteor* and *Planet* is the area of interest. The radar echoes seen by the *Oceanographer* radar are outlined.

Horizontal measurements from aircraft, vertical measurements from tethered balloons and structure sondes, surface measurements from ships and buoys, cloud field descriptions from satellite, radar and all-sky camera imagery and budget analyses are combined to describe the fair weather boundary layer on 10 September 1974. These instrumentation platforms and the budget analysis technique were employed prior to GATE but never simultaneously, (e.g., Pennell and LeMone, 1974; Echternacht and Garstang, 1976; Holland and Rasmusson, 1973; Augstein, *et al.*, 1973). It will be seen that the results of many of these individual studies are put into better perspective by combining all the strategies in one case study.

2. General weather situation

The moist convection on 10 September 1974 was suppressed across most of the GATE area for most of the daylight hours. There was extensive convection on the previous day which had severely altered the mixed layer (NSF/NCAR, 1977). However, the convection had dissipated by 0400 GMT leaving only some isolated small (not resolvable on the infrared satellite picture) cells to persist until about 0800. The visible satellite picture shown in Fig. 1 depicts the cloud cover at 1500. The picture shows that the GATE array has small non-resolvable clouds (<1 km) or none at all. Ship and aircraft observations indicate cumulus covering ~10% of the sky. Aircraft films show maximum cumulus tops at about 1100 m. The radar echoes, depicted by solid outlines in Fig. 1, show that some deep convection does exist in the southeast part of the B-scale array. This convection, associated with the extensive cloud to the southeast of the array, spreads northward but stays out of the C-scale triangle (*Dallas-Meteor-Planet*). However, the *Dallas* all-sky camera films show a patch of small cumulus and scud accompanied by rapid changes in the boundary-layer structure arriving at the *Dallas* at 1530 GMT and persisting until 1740. These clouds were too weak to show up on the *Oceanographer* or *Dallas* radar. The surface and mixed-layer winds were westerly due to an east-west ridge whose axis was at ~5°N and were backing during the afternoon from 240 to 300°. Streamline analysis for 1200 and 1800 GMT appear in Fig. 2.

3. Data sampling strategy

In response to the suppressed state of convection, the U.S. DC-6 and the U.K. C-130 flew L-shaped patterns (L1-A-L2 in Fig. 3a) from 1238 to 1605 when the DC-6 departed. From 1624 to 1746 the U.K. C-130 flew east/west patterns as shown schematically in Fig. 3a. All legs were 4–6 min in length (24–36 km) and ranged in height from 15 to 900 m. The area covered by the aircraft is illustrated in Fig. 3b.

Tethered balloon systems on the *Dallas* and *Meteor* were gathering data in a fixed-level mode throughout the day. The *Dallas* balloon system provided wind speed (V), potential temperature (θ) and specific humidity (q) at 300, 410, 550, 640 and 900 m from 1329 to 1730 GMT. The *Meteor* balloon

provided wind direction as well as V, θ and q at 200 and 400 m from 1130 to 1618.

Wind and thermodynamic soundings were taken at the *Fay*, *Meteor* and *Planet*. Surface observations are available for all the B-scale ships on an hourly basis. Based on these data, budgets of mass and the thermodynamic variables have been computed for the C-scale triangle for the period 1030–1630.

Buoy or boom surface layer wind, temperature and mixing ratio data were available on a nearly continuous basis at the *Dallas*, *Meteor*, *Oceanographer*, *Researcher* and *Quadra*. Data for the period 1200–1700 are used in this paper. It is clear from Fig. 3 and the foregoing discussion that the observations used have sufficient overlap both in space and time that they can be compared meaningfully.

4. Instrumentation and data reduction

Owing to the large number of data sources utilized in this paper and the complexity of each system, it is not possible to discuss each instrument in any detail. However, a brief outline of the fundamental characteristics of each system will be given along with references to more detailed accounts. This should acquaint the reader with the relative advantages and disadvantages and aid in the interpretation of the results.

a. Aircraft data

The data used here are from two gust probe aircraft, the U.S. DC-6 operated by the NOAA Research Flight Facility and the U.K. C-130 operated by the Meteorological Research Flight, Farnborough, U.K.

Air velocities are found by subtracking the aircraft velocity with respect to the earth from the air motion with respect to the aircraft (see Lenschow, 1972). The aircraft velocity is determined from an inertial navigation system (INS) on the U.K. C-130, and by horizontal accelerometers and an INS on the DC-6. The speed of the air moving past the aircraft is measured by a pitot-static tube; its direction is determined by means of vanes. The temperature is sensed by a Rosemount thermometer on the C-130, and by a thermistor on the DC-6. On both aircraft, water vapor fluctuations are determined by combining the output from a microwave refractometer with temperature and pressure via the refractive index equation (McGavin and Vettor, 1963). The absolute accuracy in wind velocity is on the order of 1 m s^{-1}; for temperature, 0.2 K; and for mixing ratio, 1 g kg^{-1} (Rockwood *et al.*, 1977). The mean profiles of average wind, temperature, specific humidity and fluxes of these quantities presented in this paper are based on averages over single, straight and level flight legs. Thus the profile values are means of ~24 km of data for a 4 min flight leg.

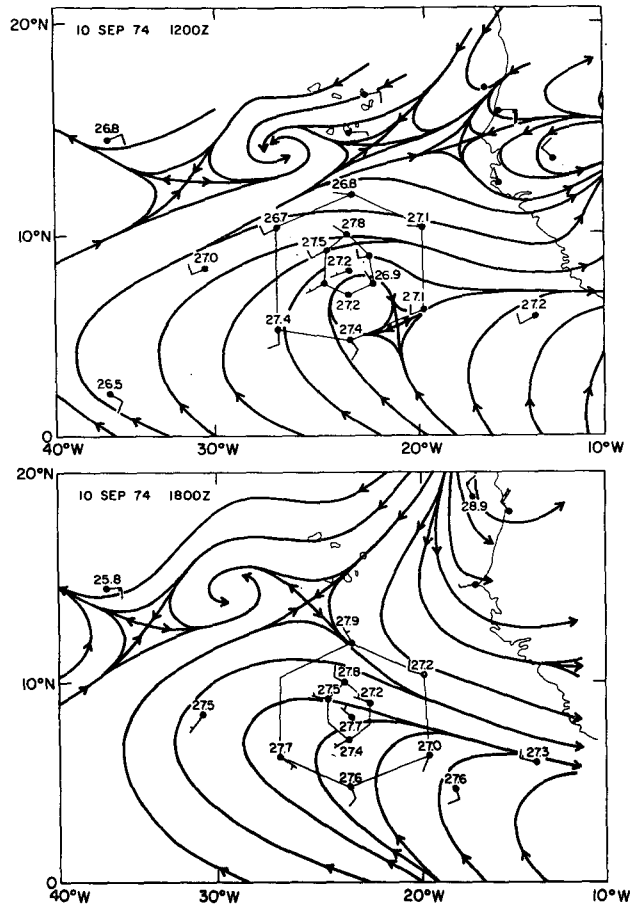

FIG. 2. Surface charts for 1200 and 1800 GMT September 1974. Thin lines outline the A/B and B ship arrays.

The flux of any quantity (b) is computed from 20 s data after removal of linear trends from vertical velocity w and quantity b. The aircraft turbulence sensing systems are both capable of measuring horizontal and vertical wind to a few cm s^{-1}, temperature fluctuations to ~0.03 K and humidity to a few hundredths of a g kg^{-1} (LeMone and Pennell, 1976). Response of the instrumentation is sufficient to resolve motions from ~10 m to several kilometers. According to Pennell and LeMone (1978), a major problem in interpreting flux data over a flight leg is atmospheric variability; the interception of a strong plume on one run is sufficient to significantly alter the average fluxes.

b. Tethered balloon data

The tethered balloon systems on the *Dallas* (Garstang *et al.*, 1977) and *Meteor* utilize sondes which were attached to the balloon's tether line. Each sonde was affixed to the tether at its center of gravity in such a way that it was free to align with the airstream. Wind speeds were measured at the

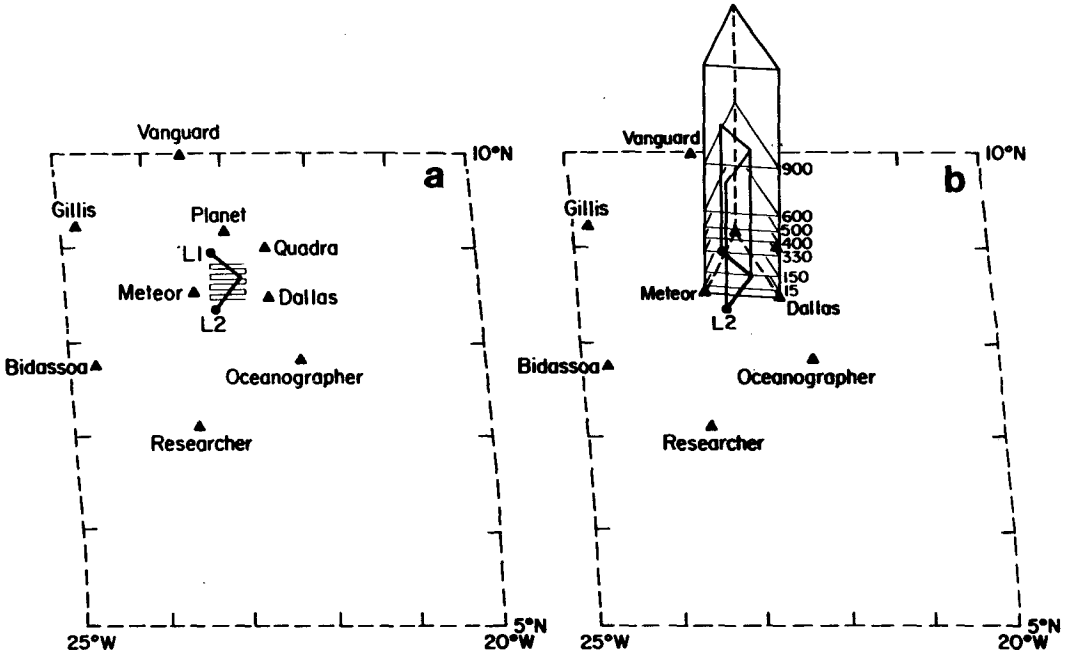

FIG. 3. Aircarft observations taken in the C-scale area. (a) The right angle pattern L1–L2 depicts the basic aircraft path: the horizontal lines show schematically the UK C-130 flight pattern from 1624 to 1746 GMT. (b) The volume covered by various observing platforms. The bold line right triangular parallelepiped represents the volume used for budget calculations; the folded sheet opening west is the area covered by the DC-6 and the UK C-130. For budgets, the time involved was 1200–1700; for aircraft, 1238–1746, including the line pattern in Fig. 3a. Heights are in meters.

windward end of each sonde by means of an impeller anemometer on the *Meteor* and by a three-cup anemometer on the *Dallas*. The wind direction was measured by referring the sonde alignment to magnetic north. Both systems measured temperatures using wet- and dry-bulb thermistors. The *Meteor* wet-bulb was fan ventilated. All temperature sensors were shielded from radiation. Pressure was measured in both cases using an aneroid capsule. For the *Meteor* and *Dallas* sondes, the estimated absolute accuracies are: wind direction, ±10°; wind speed, ±0.2 m s^{-1}; T and T_w, ±0.2 K; pressure, ±2.0 mb. Relative accuracies for both systems were much better. Relative errors between different sensors were estimated during baseline operations. Although data were sampled at rates up to 15 min^{-1}, we consider 3 min averages here.

c. Ship surface data

The "surface" (10 m) data used here for flux computations were gathered from instruments on a buoy adjacent to the *Meteor*, and from sensors affixed to booms on the prows of the *Dallas*, *Quadra*, *Oceanographer* and *Researcher*. The temperature and humidity at the boom heights were measured by wet- and dry-bulb thermistors. On the *Meteor* buoy wet and dry platinum resistance wires were used. The sensors were aspirated and shielded from radiation. Cup anemometers and wind vanes were used for wind measurements at all five locations. Sea surface temperatures were measured between 10 and 25 cm depth by thermistors attached to floats. Further detail on ship instrumentation is available in Seguin *et al.* (1978).

Surface fluxes were calculated from the aerodynamic technique, i.e.,

$$\text{sensible heat flux} = \rho c_p(\overline{w'T'}) = \overline{\rho c_p U_{10} c_H(\theta_{10} - \theta_0)}, \quad (1)$$

$$\text{latent heat flux} = \rho L w'q' = \rho L U_{10} c_E(q_{10} - q_0), \quad (2)$$

where $(\theta_{10} - \theta_0)$ and $(q_{10} - q_0)$ are the departures of the 10 m potential temperature and specific humidity from their values at the sea surface, U_{10} is the 10 m wind speed, ρ the air density, c_p the specific heat at constant pressure for moist air, and L the latent heat of vaporization for water. Each U, T and q is averaged over 10 min except for *Quadra* (30 min). The bars denote averages over the period 1200–1700 GMT. The drag coefficients ($c_H = 1.6 \times 10^{-3}$; $c_E = 1.4 \times 10^{-3}$) used were those presented at the GATE Workshop (NSF/NCAR, 1977) in a paper comparing flux to profile measurements by Hasse and Businger.

TABLE 1. Mean subcloud-layer budget of temperature in the C-scale triangle (see Fig. 3b).

$S_{10} = +S_2 + S_3 + S_4 + S_{52}$		
$S_{10} = -\frac{1}{6\tilde{\rho}c_p}\sum_{i=1}^{6}\frac{\partial\widetilde{(\bar{\rho}c_p\bar{T})}^{b,c}}{\partial t}$	+0.046 K h^{-1}	Time rate of change of T
$S_2 = -\frac{1}{6\rho c_p}\sum_{i=1}^{6}\frac{1}{F}\oint\tilde{\rho}c_p\tilde{T}\tilde{V}_n\cdot dl^{d}$	−1.50 K h^{-1}	Horizontal transport by mean flow
$S_3 = -\frac{1}{600\rho c_p}\sum_{i=1}^{6}\widetilde{\tilde{\rho}c_p\tilde{T}\bar{w}}\Big\vert_{z=0}^{z=600\text{ m}}$	+1.56 K h^{-1}	Vertical transport by mean flow
$S_4 = -\frac{1}{600\rho c_p}\sum_{i=1}^{6}\widetilde{\tilde{\rho}c_p\overline{w'T'}}\Big\vert_{z=0}^{z=600\text{ m}}$	+0.04 K h^{-1}	Vertical divergence of heat flux
$S_{52} = \frac{1}{6\rho c_p}\sum_{i=1}^{6}\widetilde{c_p\rho\left(\frac{dT}{dt}\right)_{RAD}}$	−0.05 K h^{-1}	Heating/cooling by radiation

[b] The overbar denotes a time average over T, at height z_i (z_i = 50 m, z_2 = 150 m, . . . , z_b = 550 m).
[c] The tilde denotes an average at a given height over the C-scale triangle.
[d] F is the perimeter of the triangle.
Multiply K h^{-1} by 1160/3600 to get terms in W m^{-2}.

d. Budget fluxes—computational procedure

Budgets of mass, heat and moisture were computed from high vertical resolution temperature and wind profiles obtained with structure sondes at the *Meteor*, *Planet* and *Fay* for the period 1030–1630 GMT. Three temperature and humidity profiles were obtained at each ship during this time. Seventeen wind sondes were launched during the same period: five at *Meteor*, seven at the *Fay* and five at the *Planet*. On the structure sondes the temperature, wet-bulb temperature and pressure were sampled twice a second with dry- and wet-bulb NTC resistors and an aneroid capsule. The wind profiles were derived from the radar tracking of balloons carrying a radar target at the *Meteor* and by theodolite tracking at the *Fay*, and the *Planet*.

Budgets of mass, dry static energy (s) and latent heat (Lq) were computed for an atmospheric box over the C-scale triangle for the time period $\Delta\tau$ = 1030–1630. The budget equations for s and Lq for that part of the volume in Fig. 3 bounded by the surface and cloud base are presented in Tables 1 and 2. The integration is done over 100 m layers. The surface flux is given as a lower boundary condition. Horizontal advection is by wind averaged over $\Delta\tau$. Linear variations of s, Lq and V are assumed between the vertices of the triangle. Vertical velocity $\bar{w}$ is assumed constant over $\Delta\tau$ and a function of z only. Turbulence transport at the surface is assumed equal to the bulk aerodynamic fluxes from ship surface data. Since the budgets are for the subcloud layer, the source terms are associated with radiation only. If a quantity is associated with cloudiness and cloudiness varies, the storage of the quantity in these clouds must be accounted for. The turbulence transport of the quantity at h can then be found as a residual. Detailed discussion and explicit equations can be found in Brummer (1978).

For the radiation calculation, the amount of cloudi-

TABLE 2. Mean subcloud-layer (0–600 m) budget* of specific humidity in the C-scale triangle (see Fig. 3b).

$Q_{10} = -Q_2 - Q_3 - Q_4$		
$Q_{10} = \frac{1}{6\tilde{\rho}L}\sum_{i=1}^{6}\widetilde{\rho L\frac{\partial\bar{q}}{\partial t}}$	−0.01 g kg^{-1} h^{-1}	Time rate of change
$Q_2 = \sum_{i=1}^{6}\frac{1}{F}\frac{\oint\bar{\rho}_i\tilde{L}\tilde{V}_n q dl}{6\rho L}$	+0.16	Horizontal transport by mean flow
$Q_3 = \frac{1}{600\rho L}\sum_{i=1}^{6}\widetilde{\rho L\tilde{q}\bar{w}}\Big\vert_{z=0}^{z=600\text{ m}}$	−0.055	Vertical transport by mean flow
$Q_4 = \frac{1}{600\rho L}\sum_{i=1}^{6}\widetilde{\tilde{\rho}L\overline{q'w'}}\Big\vert_{z=0}^{z=600\text{ m}}$	−0.10	Mean turbulence flux divergence

* See Table 1 for explanation of symbols.
Multiply by 2990/3600 to get W m^{-2}. g kg h^{-1} by 2990/3600 to get terms in W m^{-2}.

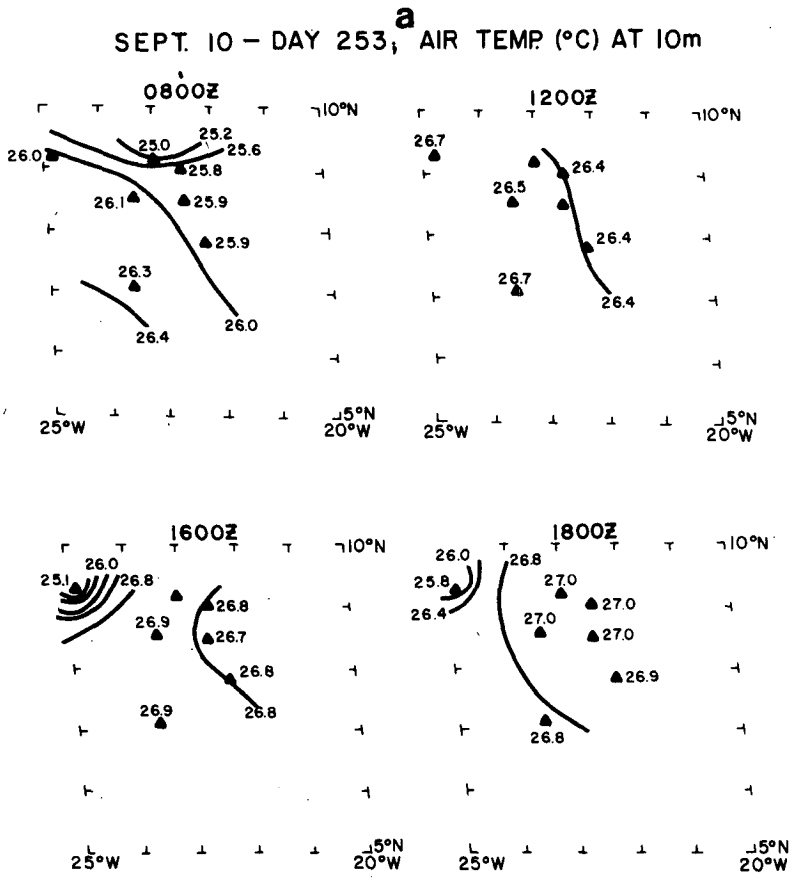

FIG. 4a. Sea surface temperature as a function of time from the boom data of the *Dallas*, *Planet*, *Researcher*, *Oceanographer*, *Quadra* and the buoy of the *Meteor*.

ness had to be known. An amount of 11% was used on hourly observations from the *Meteor*, *Fay* and *Planet* from 1000–1700. Subsequent analysis of UK C-130 upward looking IR data (Nicholls and LeMone, 1979) suggest a similar figure. Cloud base was taken as 600 m based on estimates of the LCL from surface observations and radiosonde ascents from the three C-scale ships. Aircraft photography showed a cloud base of 580 m supporting the cloud-base estimates and suggesting a mean cloud thickness of 500 m.

According to Brummer (1978) the major error in flux estimates is due to inaccuracy in measuring wind. A wind error of 1 m s^{-1} leads to a flux divergence error which accumulates at 1–3 W m^{-2} (100 m).$^{-1}$ We shall see below that other terms also contribute significantly to the total error in the flux estimates.

5. Results—Mean quantities

a. Horizontal fields

The temperature field at 10 m is shown for the GATE B-scale array in Fig. 4a. The temperatures were fairly uniform across the C-scale triangle by 1200 GMT. They increased by ~1 K from 0800–1800, about twice the average diurnal range for Phase III of GATE. The cool temperatures in the extreme northwest portion of the array are related to showers which occurred at the *Gilliss* from 1441–1515 and 1550–1625.

The specific humidity field at 10 m for the GATE B area is shown for six times on day 253 in Fig. 4b. The drier air in the west is in evidence at the *Vize* (near the *Meteor* but not shown) as well as the *Meteor*. This air is probably modified outflow from the previous day's convection, which was most intense to the west of the C-scale triangle (see NSF/NCAR, 1977). On the average the specific humidity at 10 m decreases 0.07 mg kg^{-1} h^{-1} from 0800–1600. Variation at individual locations is not monotonic. The higher q (17.1 g kg^{-1}) at the *Gilliss* at 1600 is related to light showers. An analysis of the q field within the C-scale triangle (see Fig. 3), as measured by the UK C-130 at 150 m, appears in Fig. 5. Note the apparent NW–SE dry and moist bands with ~10 km spacing. The pattern is quite dissimilar to that of the preexisting convection of 9

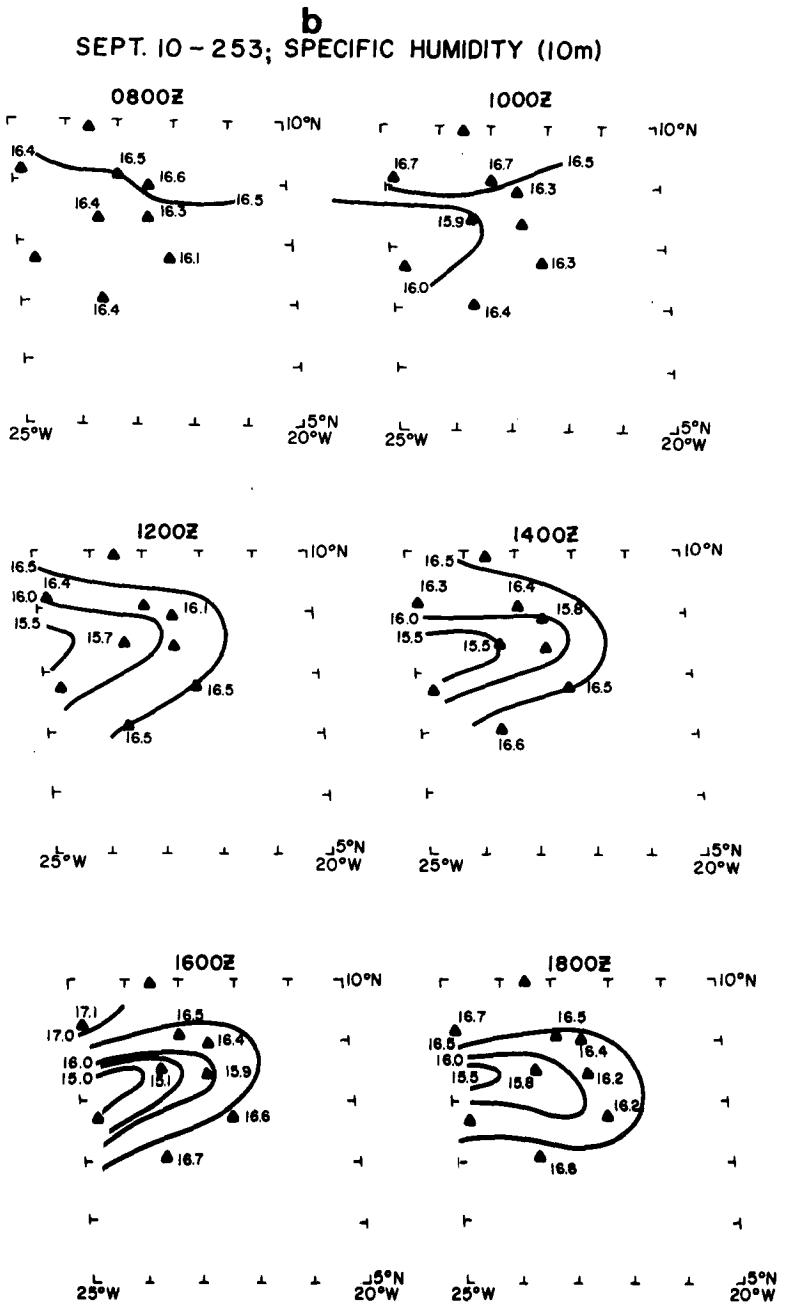

FIG. 4b. As in 4a except for air temperature at 10 m.

September. Instead, it is normal to the shear around cloud base (see Fig. 11) with correlation between moist bands and cloudiness as sensed by the UK C-130 upward looking radiometer. The banded structures in q are detectable by aircraft through the subcloud layer down to 15 m. The amplitude (0.25 g kg^{-1}) is comparable through the subcloud layer down to 15 m. The standard deviation of q (σ_q) is shown as a function of height in Fig. 6. The increase in σ_q with height above the subcloud layer is largely due to perturbations in the 1.5–3 km range.

b. Profiles

The q profiles from the *Meteor, Planet* and *Fay* appear in Fig. 7. Although there is some hint of a drying with time, the variations of the depth of the average mixed layer and the variations in q within that layer are erratic. It is suspected that the drier,

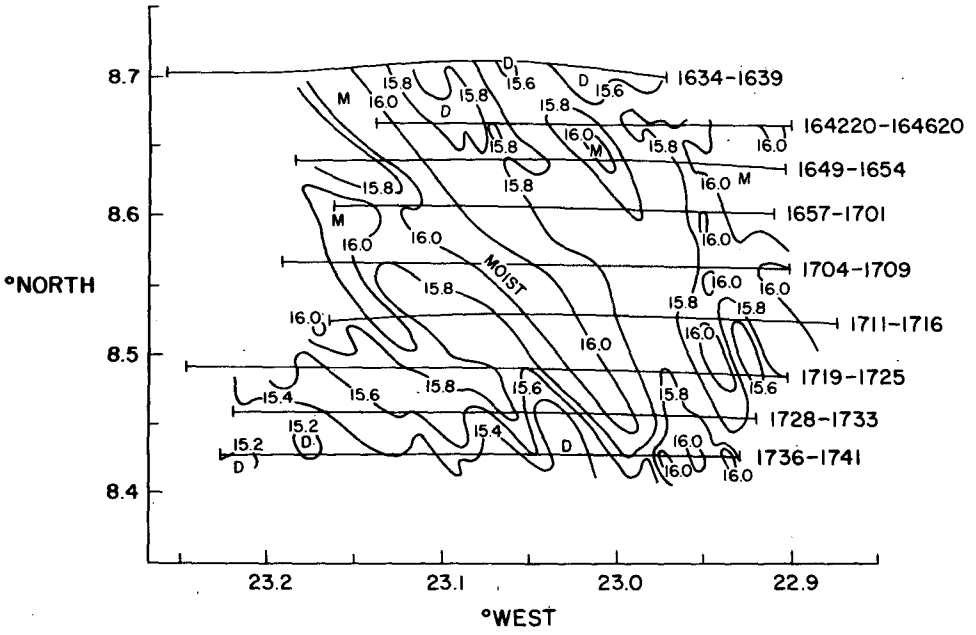

FIG. 5. Plan view of specific humidity (q) (g kg^{-1}) at 150 m as measured by the UK C-130. M, moist; D, dry.

shallower mixed-layer soundings are taken within the drier areas of the pattern appearing in Fig. 5. The average q profiles at each of the ships of Fig. 7 appear along with the average temperatures in Fig. 8. The apparent shallow mixed layer at the *Meteor* is the result of the 1329 GMT sounding.

Profiles of time- and space-averaged θ and q appear in Figs. 9 and 10. Time averages are from the *Dallas* tethered balloon (average 1329–1730) and the *Meteor* balloon (1130–1618). Time/space averages are represented by triangles for the UK C-130 (1238–1605, 1624–1736) and squares for the DC-6 (1238–1605). The solid line is the average θ (or q) from the *Fay, Planet* and *Meteor* soundings (see Fig. 8). The near-constant θ and q in the lowest 550 m is characteristic of a fair-weather boundary layer. This indicates that recovery from the previously disturbed boundary layer (Echternacht and Garstang, 1976) is essentially complete. Both θ and q profiles are within the range of "typical" fair weather days (Nicholls and LeMone, 1979). Scatter in θ is <0.25 K and for q, about 0.05 g kg^{-1}. Some of this scatter may be due to time and space variations. We shall see below that the mixed layer at the *Dallas* became more moist and more unstable at about 1530 when a group of small cumulus passed overhead.

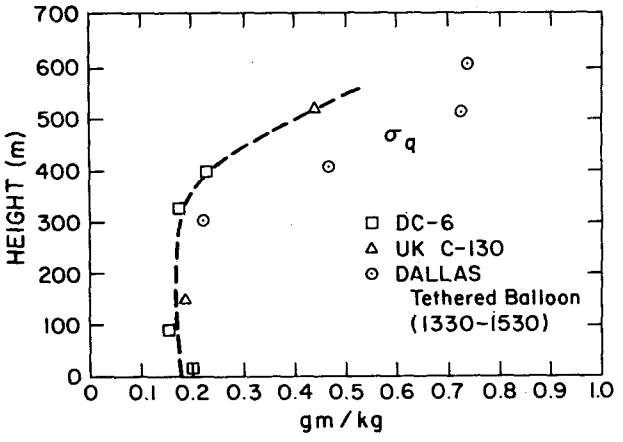

FIG. 6. Standard deviation of q as a function of height for the DC-6, UK C-130 and *Dallas* tethered balloon data.

Profiles of the wind components u (positive east) and v (positive north) appear in Fig. 11. Some of the wind variation is a function of location within the sampled volume. Integrating the divergence from the surface to cloud base (600 m) yields a vertical velocity of -4×10^{-4} m s^{-1}, a reasonable value for suppressed conditions. Since the tethered balloons were not measuring wind direction reliably on this day, the total wind speed measured by the various systems is compared in Fig. 12. The data scatter around the solid line, which represents the average from the wind sondes at the *Planet, Meteor* and *Fay*. An example illustrating the source of the scatter is the existence of a maximum at 650 m at the *Dallas* only before the convection at 1530; afterward, the wind speed did not change significantly with height. Further, the mesoscale structure in Fig. 5 affected calculations of wind means as well as those of T and q.

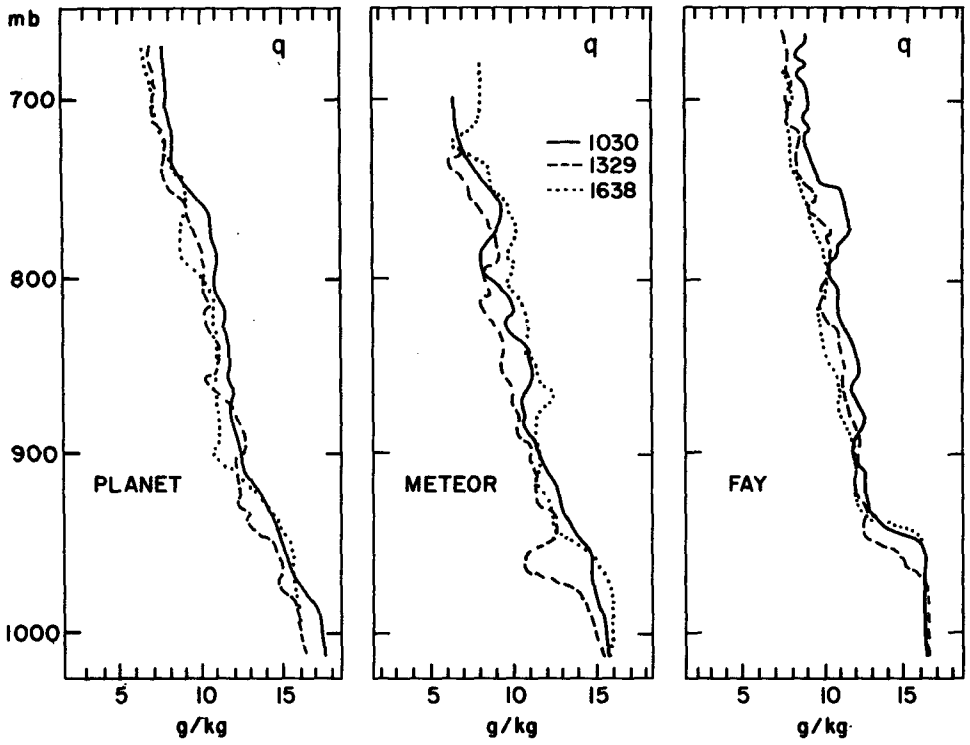

FIG. 7. Specific humidity (q) profiles for the *Planet*, *Meteor* and *Fay*.

6. Results—Time changes

a. Low-frequency changes of T and q in the mixed level

The warming of the air at 10 m has already been noted in Fig. 4a. The temperature at 10 m and the sea surface temperature (actually ~10 cm below the surface) are plotted for six ships in Figs. 13a and 13b. Since the air temperatures are from buoys (*Meteor*) or booms (other ships), the warming associated with the ship's heat island effect should be unimportant. The sea surface temperatures and their variations are close to the average for Phase III suggesting recovery from the previous disturbed day. The sea surface temperatures for all vessels except the *Quadra* increased an average of 0.8°C from 0800 to 1800. The lower values of sea surface

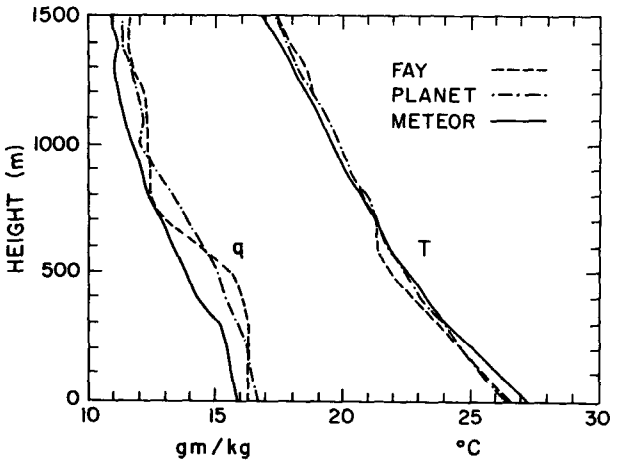

FIG. 8. Average profiles of temperature (T) and specific humidity (q) from 1030–1700 GMT and for *Fay* (3 soundings), *Meteor* (3) and *Planet* (3). See Fig. 7 for individual sounding times.

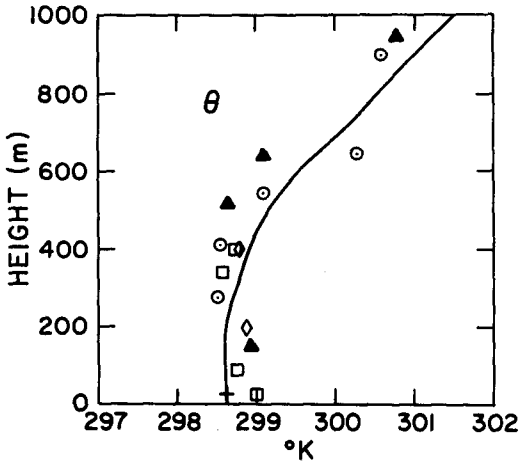

FIG. 9. Time/space averaged profiles of potential temperature (θ). German structure sondes (solid line); *Dallas* tethered balloon (⊙); DC-6 (□)/UK C-130 (▲); *Meteor* tethered balloon (◇); average *Meteor*, *Dallas* and *Quadra* surface data (+).

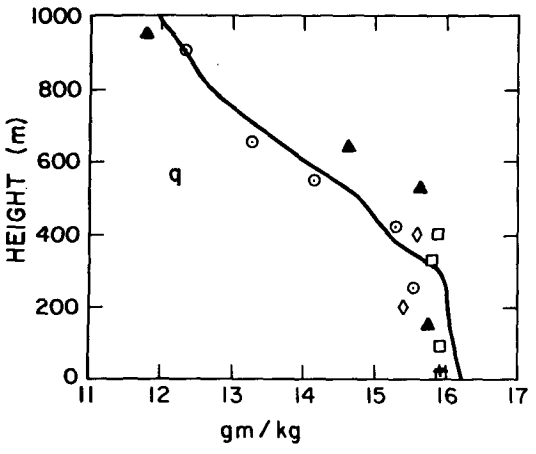

FIG. 10. Time/space averaged profiles of specific humidity (q). Symbols as in Fig. 9.

temperature measured by the automated system on the *Quadra* suggests a bias in the instrumentation. This conclusion is supported by the UK C-130 sea surface temperature mapping pattern (Fig. 3a) which suggests no north-south gradient and by the fact that the bucket temperature obtained manually at the *Quadra* agreed with that from the other vessels.

Air temperature at 10 m increased an average of 1.0°C from 0800 to 1800. The low temperature at the *Researcher* at 1400 is due to precipitation at that time. Horizontal gradients of air temperature, which existed at 0800 due to the passage of a disturbance to the north, are virtually non-existent by 1200 GMT within the C-scale triangle (Fig. 4a).

Warming was observed in the mixed layer, with drying in the western part of the triangle. From 1130–1630 the *Meteor* tethered balloon registered a temperature rise of about 1 K at 200 m (0.2 K h^{-1}) and 0.5 K at 400 m (0.1 K h^{-1}). Temperature changes at the *Dallas* were comparable with 0.2 K h^{-1} at 200 m and 0.03 K h^{-1} at 400 m. The aircraft data showed warming of 0.1 K h^{-1}. Since the aircraft data showed near constant θ with height, it is possible that the greater warming at 200 m at the *Dallas* and *Meteor* is a ship heat island effect. Hence the 400 m values (which also agree better with the aircraft trend) of 0.1 K h^{-1} seem most realistic. This is also consistent with the warming at 10 m.

The specific humidities at the two ships changed in the opposite sense with a drying (−0.1 g kg^{-1} h^{-1} at 200 m and −0.2 g kg^{-1} h^{-1} at 400 m) at the *Meteor* and a moistening (0.1 g kg^{-1} h^{-1} at 250 m and +0.2 g kg^{-1} h^{-1} at 410 m) at the *Dallas*. The surface data also show a drying near the *Meteor* and a steady or increasing q near the *Dallas*. The aircraft, flying on the average between the two locations, registered no change in q with time. This is consistent with the opposing trends along its flight paths. In the eastern part, the surface q's are steady or increasing after 1400.

b. Higher frequency time changes

A time-height crossection of q at the *Dallas* appears in Fig. 14. It is based on 75 3 min average profiles at the five sonde levels of the tethered balloon system. There is missing data between 1518 and 1530. Note the abrupt moistening about 1510. At 1530 the temperature stratification becomes more unstable; a feature which persisted for nearly 2 h. A wind maximum at 600 m prior to 1509 has already been mentioned. At 1509 the lower mixed layer winds underwent a series of small changes until there was almost no speed change with height at 1530. The changes at 1509–1530 are related to a group of small cumulus which passed over the *Dallas* at 1510.

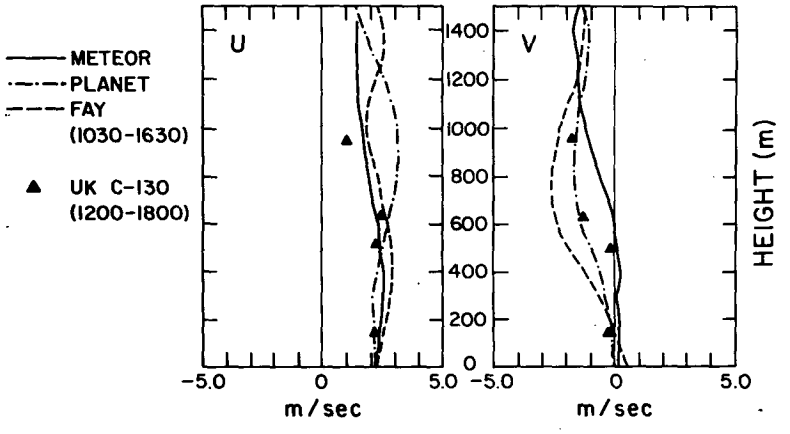

FIG. 11. Average profiles of u (positive east) and v (positive north) from 1030–1630 GMT for *Fay* (7 soundings), *Meteor* (7) and *Planet* (5). See Fig. 7 for individual sounding times. Profiles from UK C-130 taken between 1200 and 1800 are also shown.

What is the relationship of this pattern to the mesoscale pattern of Fig. 5? Advection of the moist and dry bands past the *Dallas* at the mean mixed layer speed of $(u,v) = (2.4, -0.4)$ produces oscillations of ~1.5 h period. This is not extremely different from the average time interval between the broader maxima (1415, 1530, 1620, 1720 ~1 h) or minima (1345, 1500, 1600 ~1 h). The abrupt change at 1509 clearly is due to something of larger scale which may or may not be related to the pattern. Similar changes in q appear in the *Fay* structure sonde profiles in Fig. 7.

7. Results—Fluxes

a. Direct measurements

The mean aerodynamic sensible and latent heat fluxes from 1200 to 1700 GMT for the five ships appear in Fig. 15. Note the small, apparently random variation. The first *Quadra* flux values are thought to be spurious due to poor sea surface temperature measurements by its thermistor; a second value, calculated using the bucket sea surface temperature, is included.

Aircraft latent and sensible heat fluxes are plotted along with the average of the *Dallas* and *Meteor* surface fluxes in Fig. 16. The humidity flux divergence is small and estimated to produce a q change of 0 to -0.06 kg^{-1} h^{-1}, consistent with the trend at the ships. The heat flux convergence would produce a warming of 0.06–0.08 K h^{-1}.

We can combine the potential temperature flux $\overline{w'\theta'}$ and specific humidity flux $\overline{w'q'}$ to obtain the virtual potential temperature flux $\overline{w'\theta_v'}$ from

$$\overline{w'\theta_v'} = \overline{w'\theta'} + 0.61\bar{T}(\overline{w'q'}). \quad (3)$$

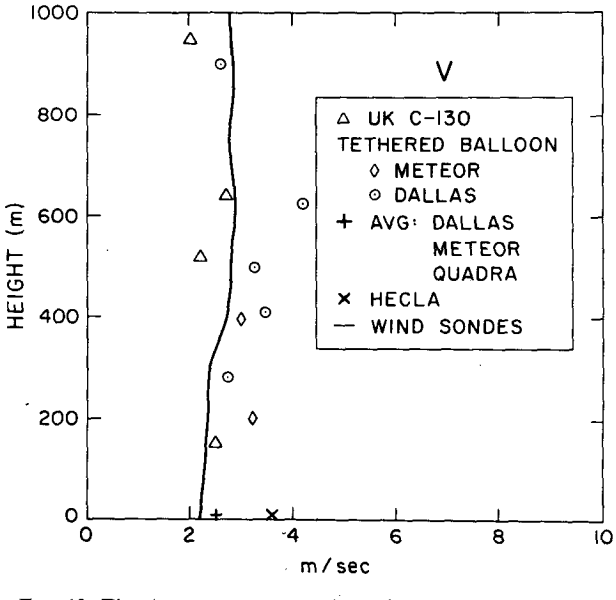

FIG. 12. Time/space average profiles of total wind speed (V).

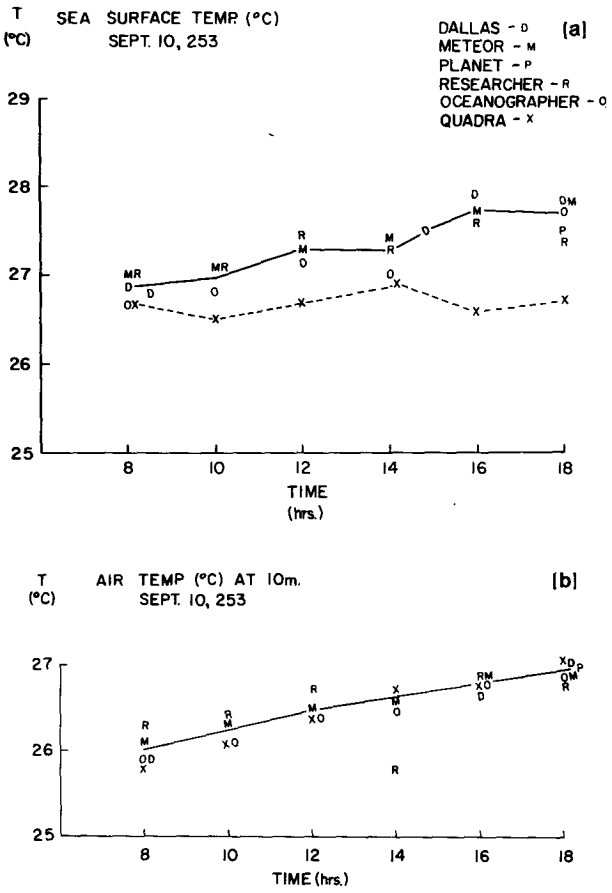

FIG. 13. (a) Fields of air temperature (°C) and (b) specific humidity (g kg^{-1}) at 10 m for the GATE B-scale area at several times between 0800 and 1800 GMT.

The resulting values at cloud base (h) and the surface (0) have a ratio $w'\theta_v'_h/w'\theta_v'_0 = -0.09$, well within the range of values Stull (1976) quotes for fair weather.

b. Budget-derived fluxes

Fig. 17 shows the fluxes of sensible and latent heat derived from the budget computations. Recall that the fluxes are found by integrating the flux-divergence term using the surface measurements as a lower boundary condition. Hence agreement must be exact at the surface. However, the budget analysis also indicated that the flux error at cloud base could be of the order of 10 W m^{-2}, if the errors in wind measurements are the major contributors to the total error in the flux estimate.

The sensible heat flux from both budget and aircraft data becomes negative well below cloud base. Humidity fluxes in both cases vary little with height below 200 m; however, the budget-derived humidity flux falls off rapidly above 200–300 m, while the directly measured aircraft fluxes are nearly con-

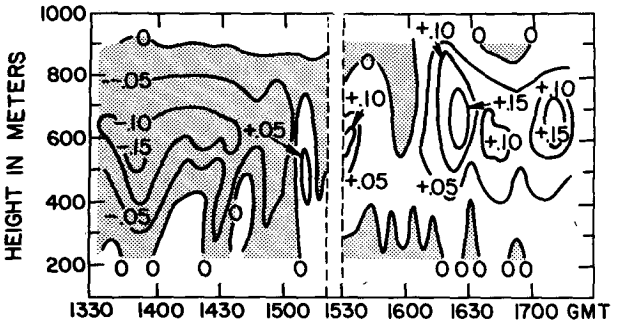

FIG. 14. Time-height cross-section of specific humidity q at the *Dallas*. Values are departures from the average at that level. Horizontal lines denote locations of the sondes. Drier areas are shaded.

stant to 500 m. Differences at cloud base are clearly greater than 10 W m^{-2}. The flux profiles are consistent with the shallower mean mixed layer heights measured by the sondes. That is, if we take the depth of the mixed layer measured by the sondes (250 m), humidity flux falloff is small and the temperature flux crosses the zero point at ~0.3 h. The crossover point for aircraft data (h = 600 m) is ~0.4 h. In an attempt to reconcile this difference, the budgets were recalculated increasing the sonde mixed-layer height to that measured by the aircraft and assigning to each additional 100 m layer the mean sonde mixed-layer value. This procedure, yielding the fluxes shown by the triangles (Fig. 17), resulted in slight but not significant improvement.

c. *Turbulence structure*

In view of the banded structure shown in Fig. 5, it is important to ask whether the q fluctuations contribute significantly to the fluxes of temperature and specific humidity. The answer is a qualified "no." To illustrate, typical cospectra for q and w and for T and w appear in Fig. 18. Each cospectra estimate is weighted by frequency so that the area in any given bandwidth is proportional to the flux by structures with frequencies in that bandwidth. For humidity, ~80% of the flux is by wavelengths 1.8 km (three times mixed layer depth, h) and smaller. However, the downward flux of heat by the banded structure is occasionally more significant.

The significance of the shorter (<3 h) wavelengths is the result of the accumulation of w energy in these same wavelengths. The wavelength of maximum energy for w increases with height in the mixed layer to a value of 1.5–2.5 h in much the same way it does in the daytime boundary layer over land (e.g., Kaimal *et al.*, 1976).

In a case study of the turbulence structure of this day, Nicholls, LeMone, and Sommeria (1980) report the turbulence energy budget to be in near equilibrium. It balances in a similar manner to that reported over land by Lenschow (1970).

8. Relating time changes to budgets

a. *Budget for the mixed layer volume*

Tables 1 and 2 summarize the results obtained from evaluating the budget equation terms averaged over the subcloud layer. The instrumentation used for the budget analysis registered a temperature increase of about 0.05 K h^{-1}. Looking at the terms of the equation, advection and vertical flux divergence contribute to the warming, with radiative flux divergence having a cooling effect.

Specific humidity remains nearly constant in agreement with the consensus trend in the C-scale triangle. The drying is a result of net advection [$-(Q_2 + Q_3)$]; the residual turbulence flux divergence cancels it out.

b. *Budget at a "point"*

The approximate equations for the time rate of change of temperature and specific humidity in a dry atmosphere are

$$\underset{1}{\frac{\partial \bar{T}}{\partial t}} = \underset{2}{-\frac{\partial}{\partial z}(\overline{w'T'})} \underset{3}{- \mathbf{V}\cdot\nabla_H \bar{T}} + R - \cancelto{0}{w\left(\frac{\partial T}{\partial z} + \frac{g}{c_p}\right)}, \tag{4}$$

$$\frac{\partial q}{\partial t} = -\frac{\partial}{\partial z}(\overline{w'q'}) - \mathbf{V}\cdot\nabla_H \bar{q} - \cancelto{0}{w\frac{\partial q}{\partial z}}. \tag{5}$$

The first term on the right is vertical flux divergence, term 2 is horizontal advection and term 3 in (4) is heating due to radiative flux divergence. The last term is vertical advection.

In the well-mixed layer, where θ, V and q are nearly independent of height, Eqs. (4) and (5) apply equally well from the surface to just below cloud base if we rewrite the vertical advection terms in the form

$$\frac{1}{h}\int_0^h w\left(\frac{\partial T}{\partial z} + \frac{g}{c_p}\right)dz \quad \text{and} \quad \frac{1}{h}\int_0^h w\frac{\partial q}{\partial z}\,dz.$$

Both of these terms are negligible for this day

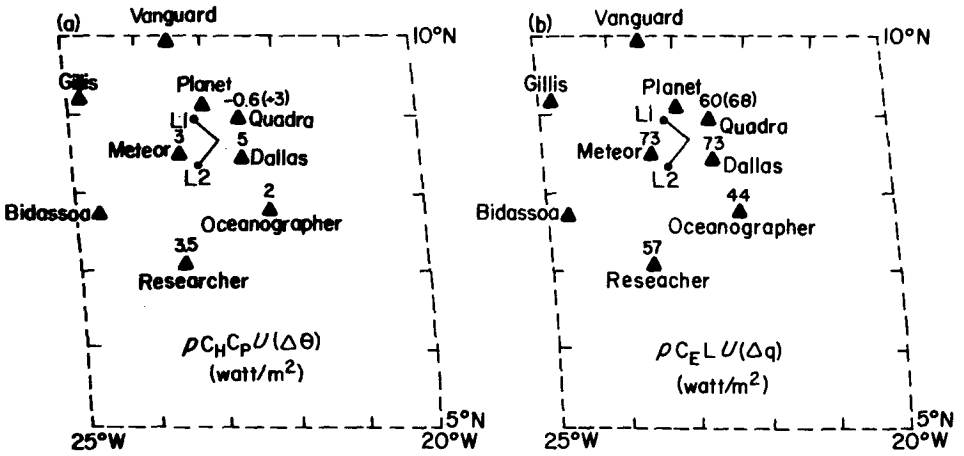

FIG. 15. Aerodynamic fluxes of (a) sensible heat (b) latent heat from the boom or buoy data of the *Dallas*, *Meteor*, *Oceanographer*, *Researcher* and *Quadra*. Fluxes using the *Quadra* bucket sea surface temperature are in parentheses.

because of the extremely small subsidence. For example, integrating the vertical temperature transport term by parts, assuming a uniform change of 1 K throughout the mixed layer, and assuming that w decreases linearly from the surface to its value at h of $\sim -4 \times 10^{-4}$ m s^{-1},

$$\frac{1}{h}\int_0^h w\left(\frac{\partial T}{\partial z}+\frac{g}{c_p}\right)dz$$

$$\approx \frac{1}{2}\left(\frac{1\text{ K}}{600\text{ m}}\times -4\times 10^{-4}\text{ m s}^{-1}\times 3600\text{ s h}^{-1}\right)$$

$$\approx 1.2\times 10^{-3}\text{ K h}^{-1}.$$

Thus we can say to good approximation that the remaining terms in (4) and (5) apply to the mixed layer averaged temperature and specific humidity.

Note that

$$\bar{\mathbf{V}}\cdot\nabla\bar{\theta}\approx\left(\mathbf{V}\cdot\nabla_H\bar{\theta}+\bar{w}\frac{\partial\theta}{\partial z}\right)_0\approx\bar{\nabla}\cdot(\bar{\mathbf{V}}\bar{\theta})$$

if $\nabla\cdot\mathbf{V}\approx 0$, and therefore that

$$\iiint\nabla\cdot\bar{\rho}\bar{\theta}\bar{\mathbf{V}}\,dxdydz=\iint\bar{\rho}\bar{\theta}\bar{\mathbf{V}}\cdot d\mathbf{l}dz.$$

Hence (4) and (5) are approximate differential forms of the more complete budget equation shown in Tables 1 and 2.

The values of the terms in (4) and (5) are shown in Table 3. Term 1 was obtained from Fig. 14. Term 2 can be obtained from combining the average T's and q's at the vertices of the C-scale triangle with u and v from Fig. 11. Two independent evaluations of Term 3 were done: the first as part of the budget computation discussed above (see Brummer, 1978); the second is from Nicholls and LeMone (1979).

For temperature, advection is apparently unimportant, in contrast to the volume budget analysis. The vertical flux divergence may be slightly small due to salt contamination of the dry bulb and the resulting high temperature readings in the near-saturated and near-cloud-base areas (Nicholls and

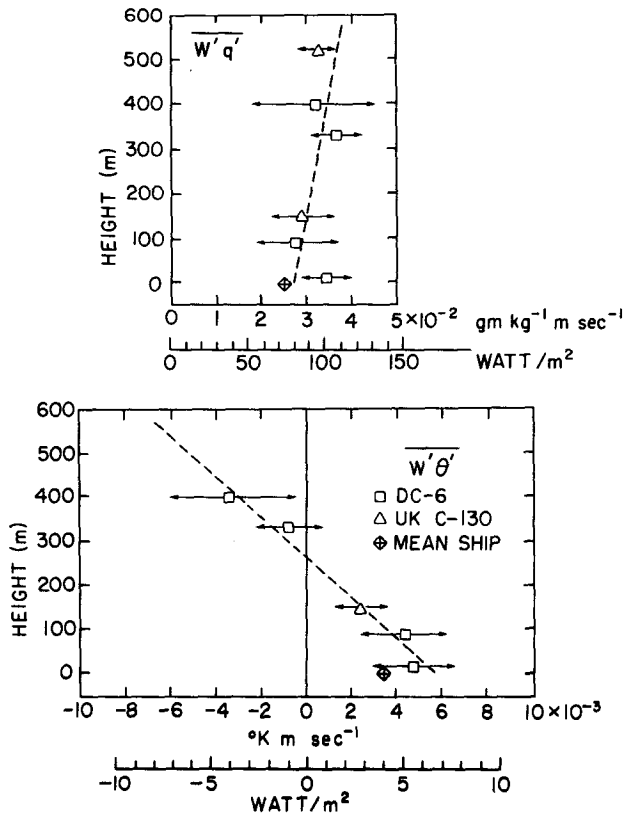

FIG. 16. Latent (top) and sensible heat (bottom) fluxes as measured by the UK C-130, DC-6 and ships boom. Scales in g kg^{-1} s^{-1} and K m s^{-1} are also given for convenience.

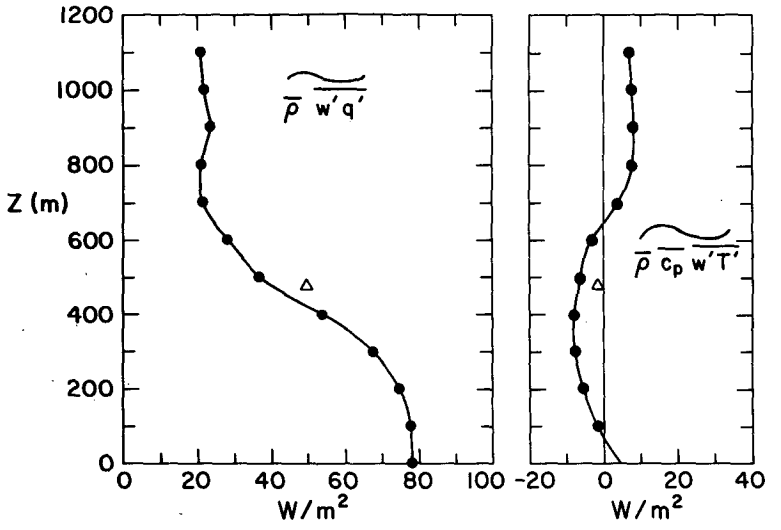

FIG. 17. Subgrid-scale (smaller than C-scale triangle) fluxes of latent heat (left) and of sensible heat (right) from budget calculations at 100 m intervals (solid line), and following top of mixed layer (single point in triangle).

LeMone, 1979). The humidity budget shows both turbulence flux divergence and advection contributing to drying.

c. A comparison

Which results are more believable? The questionable sampling of T and q by only nine soundings was already noted. But both budgets yielded a slight rise in temperature and produced the same humidity trend.

Particularly in view of the mesoscale structures of Fig. 5 and the invasion of the moist tongue at the *Dallas*, the moisture gradients will have large perturbations. Hence accounting for any linear variation between the measured values at the vertices yields little, if any, improvement of the results. That the net advection terms of the volume budget agree in sign with those of the local budget is encouraging. The first relies on the soundings, while the second assumes a uniform mixed layer with the surface θ and q gradients. Given the uncertainty of the advection in the volume budgets, the fluxes measured directly by the aircraft are more believable.

9. Discussion and conclusions

The combination of several measurement analysis strategies made possible a rather complete picture of a suppressed day. Horizontal and vertical variations of humidity and temperature in time and space suggested a complex picture. Yet the behavior of the turbulence was typical of a "horizontally homogeneous" fair weather boundary layer. The resolution of this paradox revealed some unexpected characteristics of a fair weather boundary layer. It also showed that many problems in computation and interpretations were due to atmospheric variability rather than instrumental errors.

a. Description of the mixed layer

Small cumulus covered roughly 10% of the sky with bases near 600 m. The air was, on the average, drier to the west and cooler to the north. NW–SW bands of moist and dry air were spaced at 10 km intervals across the triangle. The aircraft cloud pictures showed that clouds were concentrated over the moist bands. The scale and alignment of the bands suggested that they were not related to the strong convection of the previous day. A sudden moistening at the *Dallas*, roughly coincident with an increase in cumulus convection, was related to a moist tongue of slightly larger scale. The mixed layer increased by 200 m with the passage of this patch of cumulus.

On the average, the air in the lowest 600 m over the C-scale triangle was warming (0.1 K h^{-1}) and drying (-0.06 g kg^{-1} h^{-1}). Local and volume budgets, computed to explain the trends, suggested advection is important in the drying. The aircraft flux divergence also indicated drying. Turbulence flux divergence acted to offset the cooling by radiation, and perhaps advection, to produce warming.

Turbulence behaved according to many of the relationships characteristic of a horizontally homogeneous fair weather boundary layer. On the average, θ and q varied little from 0 to 600 m. The turbulence energy equation showed near equilibrium, suggesting that the virtual temperature flux was resolvable

by aircraft measurements and that changes in the mean flow are large compared to turbulence adjustment time. The vertical velocity eddies scale with height in the lower mixed layer, and with h in the upper mixed layer. Similarly, the cospectra of T with w and q with w peak at 2–3 h. The buoyancy flux at cloud base was ~ -0.1 times the surface value.

b. Unexpected mixed-layer behavior and its resolution

1) Large local variations of the mixed-layer depth can occur in a fair-weather boundary layer. The large fluctuations of mixed-layer depth reported for fair weather (NSF/NCAR, 1977) was considered questionable by the aircraft scientists who found the convolutions in the top of the mixed layer to be shallow and small in horizontal extent. Tethered balloon and structure sonde T and q soundings revealed uniform θ and q in layers ranging from 300 to 600 m. The classical definition of mixed layer depth (Malkus, 1958) states that its top occurs in the kink in the θ or q profile. The height of this kink may vary from profile to profile. However, for comparison of mixed layer properties, an average h is more appropriate.

2) Mesoscale structure can exist in a fair weather boundary layer. The 10 km moist and dry bands are associated not only with clouds, but are evident in spectra of u, v and T as well. The transport by the motions in this band width account for up to 20% of the humidity flux and possible greater fraction of the temperature flux.

3) Since such structures can exist, it is suspected that much of the scatter in fair weather data originally thought to be "instrumental" may be due to real mesoscale variation.

Acknowledgments. The GATE Workshop provided us with the opportunity to compare the data sets involved and outline the objectives of the comparison. B. Brummer computed the budgets. G. D. Emmitt and B. Brummer are responsible for the tethered balloon data for the *Dallas* and *Meteor*, respectively. G. Barnes computed the surface fluxes. S. Nicholls, W. T. Pennell and M. LeMone did the computation of the aircraft fluxes. LeMone compiled the data and remarks and wrote the first draft of the paper.

We gratefully acknowledge the sincere effort and spirit of cooperation of the many people involved in taking these observations. No less important was their effort in editing the data and putting it into a form which makes productive analysis possible.

This work was partially supported by the Global Atmospheric Research Program, National Science Foundation and the U.S. GATE Project Office, National Oceanic and Atmospheric Administration, under Grant ATM74-21701.

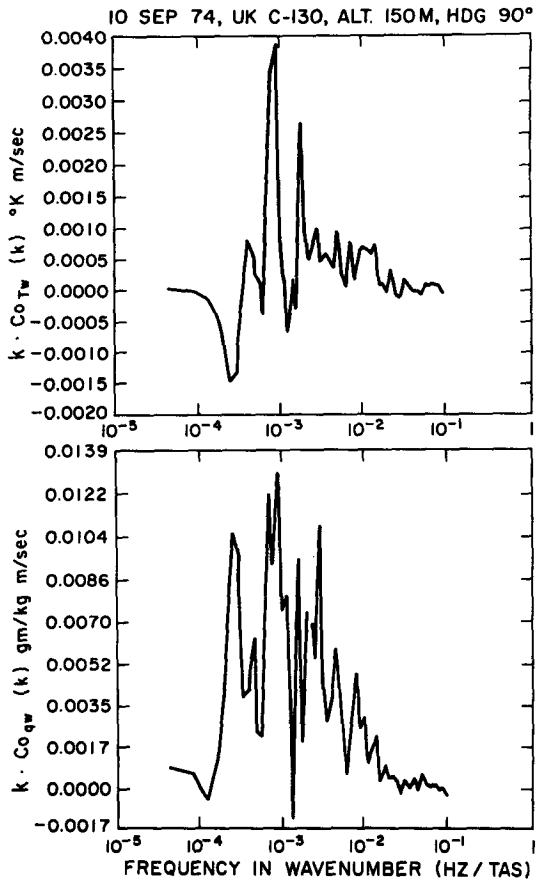

FIG. 18. Frequency-weighted cospectra of (a) T and w, (Co_{Tw}) and (b) q and w, (Co_{qw}) at 150 m for the UK C-130.

TABLE 3. Evaluation of terms in temperature and humidity change equation, in a vertical column of height h.

	Vertical flux divergence (Term 1)	Horizontal advection (Term 2)	Radiative flux divergence (Term 3)	Time change
T	0.06–0.08 K h^{-1}	−0.01 K h^{-1}	−0.05 K h^{-1}*	+0.1 K h^{-1}
q	0–0.06 g kg^{-1} h^{-1}	−0.026 g kg^{-1} h^{-1}	−0.04 K h^{-1}**	0 → 0.07 g kg^{-1} h^{-1}

* From Table 1.
** See Nicholls and Le Mone (1979).

REFERENCES

Augstein, E., H. Riehl, F. Ostapoff and V. Wagner, 1973: Mass and energy transports in an undisturbed Atlantic trade wind flow. *Mon.Wea. Rev.*, **101**, 101–111.

Brummer, B., 1978: Mass and energy budgets of a 1 km high atmospheric box over the GATE C-scale triangle during undisturbed and disturbed weather conditions. *J. Atmos. Sci.*, **35**, 997–1011.

Echternacht, K. L., and M. Garstang, 1976: Changes in the structure of the tropical subcloud layer from the undisturbed to disturbed states. *Mon. Wea. Rev.*, **104**, 407–417.

Garstang, M., G. D. Emmitt, G. Barnes, D. Fitzjarrald, E. Tollerud and J. D. Brown, 1977: The U.S. GATE Tethered Balloon Systems: A discussion of the measurements. Part 3 of Report 2, Cloud Populations and Their Interaction with the Boundary Layer. NSF Grant ATM74-21701 and Final Report under NOAA Contract 04-6-158-44067. [Available from the Department of Environmental Sciences, University of Virginia, Charlottesville, VA 22903.]

Holland, J. Z., and E. Rasmusson, 1973: Measurements of the atmospheric mass, energy and momentum budgets over a 500 km square of the tropical ocean. *Mon. Wea. Rev.*, **101**, 44–55.

Kaimal, J. C., J. C. Wyngaard, D. A. Haugen, O. R. Coté, Y. Izumi, S. J. Caughey and C. J. Readings, 1976: Turbulent structure in the convective boundary layer. *J. Atmos. Sci.*, **33**, 2152–2169.

LeMone, M. A., and W. T. Pennell, 1976: The relationship of trade wind cumulus distribution to subcloud layer fluxes and structure. *Mon. Wea. Rev.*, **104**, 525–539.

Lenschow, D. H., 1970: Airplane measurements of planetary boundary layer structure. *J. Appl. Meteor.*, **9**, 874–884.

——, 1972: The measurement of air velocity and temperature using the NCAR Buffalo aircraft measuring system. NCAR-TN/Edd-74, 30 pp.

McGavin, R. E., and M. J. Vetter, 1963: *Humidity and Moisture: Measurement and Control in Science and Industry*, Vol. 2, A. Wexler, Ed. Reinhold, 553–560.

Malkus, J. S., 1958: On the structure of the trade-wind moist layer. *Pap. Phys. Oceanogr. Meteor.*, M.I.T. and W.H.O.I., No. 13, 47 pp.

National Science Foundation and National Center for Atmospheric Research, 1977: Report of the U.S. GATE Central Program Workshop. [Available from Publications Office, NCAR, P.O. Box 3000, Boulder, CO 80307.]

Nicholls, S., and M. A. LeMone, 1980: The fair weather boundary layer in GATE: The relationship of subcloud fluxes and structure to distribution and enhancement of cumulus clouds. Submitted to *J. Atmos. Sci.*

——, —— and G. Sommeria, 1980: The simulation of a fair weather marine boundary layer in GATE using a three-dimensional model. Submitted to *Quart. J. Roy. Meteor. Soc.*

Pennell, W. T., and M. A. LeMone, 1974: An experimental study of turbulence structure in the fair weather trade wind boundary layer. *J. Atmos. Sci.*, **31**, 1308–1323.

——, 1978: An intercomparison of turbulence measurements from aircraft. To be submitted to *J. Appl. Meteor.*

Rockwood, A. A., A. H. Miller, C. E. Duchon and A. J. Koscielny, 1977: Analysis and results from the GATE tower flybys and aircraft intercomparisons of the thermodynamics variables from the U.S. Electra, DC-6, and the U.K. C-130. [Available from the U.S. GATE Project Office, NOAA/EM-6, Rockville, MD 20852.]

Seguin, W. R., R. B. Crayton, P. Sabol and J. W. Carlile, 1978: GATE Convection Subprogram Data Center: Final Report on Ship Surface Data Validation. NOAA Tech. Rep. EDS-25.

Stull, R. B., 1976: The energetics of entrainment across a density interface. *J. Atmos. Sci.*, **33**, 1260–1267.